Title

Estimation of load conditions and strain distribution for in vivo murine tibia compression loading using experimentally informed finite element models.

Authors

Pickering, Edmund

Silva, Matthew

Delisser, Peter

et al.

Publication Date

2021-01-22

DOI

10.1016/j.jbiomech.2020.110140

Peer reviewed

HHS Public Access

Author manuscript

J Biomech. Author manuscript; available in PMC 2022 January 22.

Published in final edited form as:

J Biomech. 2021 January 22; 115: 110140. doi:10.1016/j.jbiomech.2020.110140.

Estimation of load conditions and strain distribution for *in vivo* murine tibia compression loading using experimentally informed finite element models

Edmund Pickering[1,✉], **Matthew J. Silva**[2,3], **Peter Delisser**[4,5], **Michael D. Brodt**[2], **YuanTong Gu**[1], **Peter Pivonka**[1]

[1]School of Mechanical, Medical and Process Engineering, Queensland University of Technology (QUT), Brisbane, QLD 4000, Australia

[2]Department of Orthopaedic Surgery, Musculoskeletal Research Center, Washington University, Saint Louis, Missouri, USA

[3]Department of Biomedical Engineering, Washington University, Saint Louis, Missouri, USA

[4]University of Bristol School of Veterinary Science, Bristol, UK

[5]Veterinary Specialist Services, Brisbane, QLD, Australia

Abstract

The murine tibia compression model, is the gold standard for studying bone adaptation due to mechanical loading *in vivo*. Currently, a key limitation of the experimental protocol and associated finite element (FE) models is that the exact load transfer, and consequently the loading conditions on the tibial plateau, is unknown. Often in FE models, load is applied to the tibial plateau based on inferences from micro-compututed tomography (μCT). Experimental models often use a single strain gauge to assess the three-dimensional (3D) loading state. However, a single strain gauge is insufficient to validate such FE models. To address this challenge, we develop an experimentally calibrated method for identifying the load application region on the tibial plateau based upon measurements from three strain gauges. To achieve this, axial compression was conducted on mouse tibiae ($n = 3$), with strains gauges on three surfaces. FE simulations were performed to compute the strains at the gauge locations as a function of a variable load location. By minimising the error between experimental and FE strains, the precise load location was identified; this was found to vary between tibia specimens. It was further shown that commonly used FE loading conditions, found in literature, did not replicate the experimental strain distribution, highlighting the importance of load calibration. This work provides critical insights into how load is transferred to the tibial plateau. Importantly, this work develops an experimentally informed technique for loading the tibial plateau in FE models.

✉Corresponding author: ei.pickering@qut.edu.au.

Conflict of interest statement

The authors have no conflicts to report.

Keywords

Mouse tibia loading; Strain gauging; Finite element modelling; Bone mechanics; Bone adaptation

1 Introduction

Theories of bone adaptation suggest a link between the local bone (re)modelling response and the engendered stresses/strains on the bone surfaces (Frost, 2003; Rosa et al., 2015). In particular, studies have tested the hypothesis that regions of high mechanical stress/strain predict locations of new bone formation (Moustafa et al., 2012; Pereira et al., 2015). However, during *in vivo* loading studies, load alignment and misalignment have been identified as challenges (Goff et al., 2014; Main et al., 2020). In particular Goff *et al.* (2014) demonstrated the effect of misalignment in the rodent tail loading model. The significance of misalignment in other loading models is still a matter of debate.

The murine tibia compression model (De Souza et al., 2005) is the gold standard for the *in vivo* study of bone adaptation due to mechanical loading, and is used to investigate factors such as exercise (De Souza et al., 2005), age (Lynch et al., 2011), genetic makeup (Saxon et al., 2011), drugs (Sugiyama et al., 2008) and disease (Fritton et al., 2008). In this model, a controlled load is applied to the tibia through custom loading cups placed over the knee and tarsus (Main et al., 2020). Generally, loads are physiologically realistic and involve multiple loading cycles over a time course so as to induce an adaptive response. It should be noted that the tibia has no direct contact with the loading cups, since the load is applied through the distal femur and the flexed tarsus. As such, the load alignment on the tibia is not directly controlled, and can be expected to vary both intra-study (e.g. through uncontrollable experimental factors) and inter-study (e.g. through different cup designs, genomic variations, etc). Generally, single axis loads cells are used, and thus only the vertical component of the applied load is known (not the transverse component). Generally, a single strain gauge, attached to the antero-medial surface, is used to assess the state of strain (Lynch et al., 2011; Saxon et al., 2011).

The challenge of load alignment, and how load is transferred to the tibia, is relevant when considering FE models. Typically, in conjunction with *in vivo* studies, many works use FE modelling to gain deeper insights into the local mechanical stresses/strains, and how these affect adaptation (Moustafa et al., 2012; Willie et al., 2013; Yang et al., 2014; Razi et al., 2015; Albiol et al., 2019). However, the results of these FE models can be highly dependent on the boundary conditions (BCs) used (i.e. how the tibia is loaded), and the appropriateness of these BCs (Yang et al., 2014; Razi et al., 2014). It should be noted that without detailed knowledge of soft tissue interaction between the tibia and femur, the true *in vivo* loading conditions remain unknown.

As a proxy, standard loading conditions are generally employed. One common approaches is to use μCT to identify the contact areas at the tibia-femur and tibia-talus interface (Yang et al., 2014; Carriero et al., 2018; Razi et al., 2015). In the murine tibia compression model, the knee is generally at high flexion, and as such μCT shows the tibia-femur contact occurring at the posterior edges of the condyles. In FE models, load is thus distributed across these

contact points. While a powerful approach, this is limited because μCT only provides information on geometry, not on the load distribution. Thus, it is common to assume that the load is evenly distributed between the two condyles. In fact, this is often not the case; multiple studies have shown a non-even load distribution between the condyles (Borges et al., 2014; Imhauser et al., 2019; Zhang et al., 2019). As such, this assumption will likely lead to differences between the *in silico* and *in vivo* strain distributions. While μCT informed BCs are the most common, they are not the only approach. Alternatively, the interaction between the tibia and femur can be neglected and instead load can be applied evenly across either the proximal or distal articular surface of the tibia (Christiansen et al., 2008). As this loading is not physiologically realistic, it will likely lead to errors. In both cases, error between the modelled *in silico* and true *in vivo* strain distributions could lead to incorrect conclusions.

As is clear, these one-size-fits-all approaches to BCs are limited, either because they don't effectively represent the expected experimental tibial loading (i.e. applying an even load distribution) or because they don't consider variance in load alignment. Instead, an experimentally informed BC approach is required. To meet this challenge, we propose a new approach for identifying loading conditions on the tibial plateau in the murine tibia compression model. In this approach, multiple strain gauges are attached to the tibia (37% section, measured superior to inferior), and in conjunction with FE modelling, an equivalent load on the tibial plateau is determined which replicates the measured strain distribution. *Ex vivo* axial compression of tibia specimens was conducted with strain gauges attached to the the antero-medial, posterior and lateral surfaces of the tibia. Additionally, an FE model of the tibia was constructed from μCT. In the FE model, based on Saint-Venant's principle, the load on the tibial plateau was idealized as a single equivalent point load, with a variable load location (i.e. alignment). By investigating different load locations, and minimizing the error between the *ex vivo* and *in silico* strains, we were able to precisely identify the equivalent load location. This strategy was then compared to other loading strategies found in literature, where it was shown that these other strategies did not replicate the *ex vivo* strain measurements, resulting in large deviations between the experimental and *in silico* strains. The end result of this work is a reliable and experimentally informed approach to applying loads to FE models of the murine tibia compression model; a notable improvement upon previous techniques.

2 Materials and methods

2.1 Animals

This work used strain gauge and μCT data from a previously reported study (Patel et al., 2014). Data from three, five month old female C57BL/6 mice (Aged Rodent Colonies, National Institute of Ageing, NIH) was used. Upon arrival, the mice were housed for one week, then euthanised via CO_2 asphyxiation and stored at −20°C. Prior to experimentation, the bodies were thawed to room temperature. All methods used were consistent with NIH guidelines for the care and use of laboratory animals and were approved by the Washington University Animal Studies Committee.

2.2 Ex-vivo loading and strain measurements

For strain measurements, three trimmed, single-element strain gauges (C2A-06–015LW-120, Vishay Micro-Measurements) were attached to the antero-medial, lateral, and posterior surfaces of the right tibia. The gauges were aligned axial to the tibia and were attached at the 37% location (i.e. 37% along the tibia shaft, proximal to distal). To attach the gauges, the surrounding muscle and the periosteum was removed and the bone surface cleaned. The gauges were bonded to the surface using a cyanoacrylate adhesive. To verify gauge placement, μCT (70 kV, 11 μA, 100 ms integration time, 21 μm isotropic voxel size, VivaCT 40; Scanco Medical) was recorded as shown in Figure 1a. The gauge labelling used in this work is shown in Figure 1b. As the periosteal surface at the 37% section is approximately normal to the axial direction, it was assumed that the strain readings from these gauges corresponded to the axial strain within the tibia.

The mouse hindlimb was loaded within a servohydralic materials testing machine (Instron Dynamite 8800 machine with a Lebow model 3397; ± 0.1 N accuracy load cell) with cups to support the knee and tarsus. A compressive preload of 0.5 N was applied, followed by cyclic loading using a triangular function. Ten load cycles were applied with a peak load of 3 N. The load/unload rate was 80 N/s and between each cycle a 10 s rest period was used. During cycling, strain data was acquired using a signal conditioner and amplifier (SCXI-1001; National Instruments). Both strain data and load data was collected at 60 Hz (LabVIEW 9.2; National Instruments). Strain data for each of the three gauges was averaged across the final eight loading cycles (over which strain amplitudes were steady). This protocol was then repeated for peak loads of 5, 7, 9, and 11 N. The strain data for this study, along with further details of the *ex vivo* loading, has been previous published (Patel et al., 2014).

2.3 Micro-CT & FE modelling

Prior to attaching strain gauges, the geometry of the tibia was recorded via μCT (70 kV, 11 μA, 100 ms integration time, 21 μm isotropic voxel size, VivaCT 40; Scanco Medical). A voxel size of 21 μm has previously been demonstrated valid for FE modelling of mouse tibiae (Patel et al., 2014). The μCT data was outputted as a DICOM file and transfered from St. Louis to Brisbane. The FE modelling and analysis described here are new and distinct from those described by Patel *et al.* (2014).

An, automated in-house MATLAB code was used to build a 3D model of the tibia. First the μCT was segmented via thresholding using a threshold value determined via the Otsu method (Otsu, 1979). This resulted in a 3D binary object. This was cleaned via an island removal filter which removed all but the largest voxel island (determined via voxel face connectivity). Figure 1 of the Supplementary Information shows the result of this process. To create a repeatable coordinate system, the principal axes of the binary object were calculated and the longitudinal principal axis was aligned with the z axis. Following, the intercondylar notch of the tibia was aligned to the x axis. The origin of this axis was then positioned to coincide with the ankle support point, identified as the centre of the inferior articular surface. The resulting coordinate system can be seen in Figure 2a.

Soft tissue, such as at the growth plates and tibio-fibular joint, is not captured by μCT, but may affect the model. To account for this, approximate regions of the growth plates were identified and filled with voxels representative of soft tissue. This process was repeated for the soft tissue of the tibio-fibular joint. This was then converted into an FE model using a direct voxel-to-element meshing approach was used, in which each voxel was converted to an eight node solid structural element (SOLID185). Figure 2 of the Supplementary Information shows the developed mesh, including the bone and soft tissue elements.

Linear-elastic material properties were selected to match other works (Yang et al., 2014; Pereira et al., 2015; Razi et al., 2015; Moustafa et al., 2012). Bone elements were assigned an elastic modulus of 17 GPa and a Poisson's ratio of 0.3. Soft tissue of the growth plates and tibio-fibular joint were assumed to have similar properties and assigned an elastic modulus of 10 MPa and a Poisson's ratio of 0.3. The model's sensitivity to soft tissue material properties was tested and it was found the axial strain at the 37% location (i.e. strain gauge attachment site) was insensitive to these. This matches the findings of Pereira *et al.* (Pereira et al., 2015). Thus, further consideration was not given toward the soft tissue.

A schematic representation of the FE BCs is shown in Figure 2b. During *in vivo* loading, load is transferred from the inferior articular surface of the tibia to the head of the talus. It is common to assume this joint acts like a pin support (Yang et al., 2014; Pereira et al., 2015; Razi et al., 2015). To model this, nodes in the lower 10% of the tibia were constrained to a point located at the centre of the inferior articular surface (henceforth referred to as the ankle support point), which was fixed in translation directions (while allowing rotation). The ankle support point was identified from the μCT scan, inline with other studies (Yang et al., 2014; Pereira et al., 2015; Razi et al., 2015). Note, due to Saint-Venant's principal this 10% parameter is not critical, this was tested and the model was confirmed insensitive to this parameter.

The loading conditions on the tibial plateau are more complex. Here, the femur interfaces with, and applies load to, the condyles of the tibia. The load distribution developed is complex and depends on the interaction of the tibia, femur and surrounding soft tissue (Borges et al., 2014; Imhauser et al., 2019; Zhang et al., 2019). Instead of considering this complex load distribution, we argue that for analysis of the diaphysis, the load on the tibial plateau can be simplified to a single equivalent point load, acting at a representative location. The challenge is thus identifying this equivalent point of action. To this end, the FE model was designed to allow varying of the load location. A load point (P) was centred at coordinates of (x, y) (as shown in Figure 2a) on a load plane defined by the 3% slice (proximal to distal). Nodes within a 105 μm radius (i.e. 5 voxel radius) of the load point were fixed to the load point using rigid beam elements. A compressive load of $P = 10$ N was applied to the load point. During *ex vivo* loading the tibial plateau is prevented from translating in the x and y directions, while rotation is allowed. To represent this, the load point was fixed in the x and y directions. It should be noted that idealising the load distribution of the tibial plateau as a single point load is based upon St-Venant's principle. This will not be valid for regions near the load application point, but will be valid for regions within the diaphysis. This assumption was tested and confirmed for the FE model.

A grid pattern of 80 load locations on the load plane was investigated (see Figure 3 of Supplementary Information). Each load location was simulated individually using the Ansys FE package (Ansys Mechanical APDL version 18.2) under linear-elastic conditions. Following simulation, the stress and strain tensor values at the centroid of each element were exported. The equivalent strain gauge reading from the FE model was determined by averaging the axial strains (i.e. z-direction strains) of voxels at the strain gauge locations, identified from μCT (see Figure 1a).

2.4 Comparison of loading strategies

The loading strategy developed in this paper was compared to two common loading strategies found in literature. In load strategy 1 (experiment informed), load was applied to the tibial plateau, at the equivalent load location determined in this work. Load strategy 2 (μCT informed) simulated the common approach of applying load to the posterior edge of the condyles (Yang et al., 2014; Pereira et al., 2015; Razi et al., 2015; Carriero et al., 2018), as is common, it was assumed load was evenly distributed across the two condyles. To represent this strategy, an equivalent load was applied to a point, midway between the two condyles, aligned to the posterior edges of the condyles. Load strategy 3 (uniform distribution), simulated load being evenly distributed over the tibial plateau. While not representative of physiological loading, this approach is found in several studies (Christiansen et al., 2008; Oliviero et al., 2017). To represent this, an equivalent load was applied to the centroid of the 3% slice.

3 Results & discussion

In this work, three mouse tibiae were studied. For conciseness, results for specimen 1 are reported below. Results of specimen 2 and 3 are presented in the Supplementary Information.

3.1 Ex vivo loading & strain gauge data

Strain gauge data from the *ex vivo* loading is shown in Figure 3 along with linear trends. As expected, the load-strain relationship is highly linear, indicative of a linear-elastic system. Strain gauges can be expected to have an offset, which is seen in all three gauges as a non-zero strain reading at zero load. This was corrected for by subtracting the offset error. The reminder of this paper will use strain gauge values following offset subtraction.

Both the lateral and posterior gauges are under compression while the antero-medial gauge is under tension. The strain reading on the posterior surface sits within a similar range to other studies with C57BL/6 mice of a similar age (Stadelmann et al., 2009; De Souza et al., 2005; Sugiyama et al., 2008), likewise for the lateral gauge (De Souza et al., 2005). Such comparison is not possible for the posterior gauge as no previous studies have reported strain gauge readings on the antero-medial surface due to the complexity of attachment.

3.2 FE strain gauge data and determination of load location

A comparison of the experimental and FE strain gauge readings is shown in Figure 4; this figure has been developed to concisely compare and understand the effect of load location

on strain measurements. Figure 4a–c, shows a contour plot of *in silico* strain gauge reading determined through the FE model, for a 10 N compressive load, applied at a given (x,y) coordinate in $\mu\varepsilon$, for specimen 1. The red lines indicate where the FE gauge readings matches the experimental value.

From these results, it is clear that strain readings are highly sensitive to load location. A small change in load location can result in a large change in the measured strain. This highlights the importance of calibrating the experimental loading procedure to ensure the effect of experimental variations are minimised. Next, it is apparent that the locus of load locations which give a FE strain reading matching the experimental is represented by a linear line (shown in red). For all three gauges, these loci appear to converge on the lateral-posterior edge of the medial condyle.

Figure 4d shows the mean of the relative error between the experimental and FE strain gauge readings for specimen 1. This error reaches a minimum of 2.5% at a load location of (1.13,−0.42) mm (indicated by the red star). This coincides with the lateral-posterior edge of the medial condyle. Thus, this is predicted to be the equivalent load location for this model. Crucially, it can be seen that as the load deviates from this location, the error increases significantly. For example, if the load location was to shift approximately 0.2 mm in the lateral direction, this error would increase to 20%. It should be noted that as there are three strain gauges and two variables (i.e. x and y), this problem is overdetermined. As the error successfully minimises, this provides certainty that the determined load location is valid.

The predicted load location both matches and challenges common assumptions in FE modelling of the murine tibia compression model. First, due to the high knee flexion in the murine tibia compression model, it is commonly assumed that load is applied to the posterior edge of the condyles (Yang et al., 2014; Pereira et al., 2015). This assumption is supported by the predicted load location. However, it is also common to assume that the load is distributed evenly between the two condyles, this is not supported by the predicted load location, in which the load is distributed toward the medial condyle.

Rather than suggesting this is a general result, we submit that this load location is specific to the experimental setup and specimen. The exact load location will likely shift based upon experimental factors; for example, the alignment of the hindlimb within the loading apparatus, the flexion of the hindlimb during loading, or the design of the cups which secure the ankle and knee. In line with this, Figure 4e–f shows the predicted load locations of specimen 2 and 3 respectively. As expected, these locations vary for each specimen, highlighting the benefit of calibrating the load location to the experimental strain gauge readings. By calibrating the load location, confidence is achieved in the *in silico* strain distribution. A promising avenue for future studies would be to use a larger dataset to produce a statistical map of expected load locations.

3.3 Comparison of loading strategies

To further demonstrate the importance of experimentally informed loading conditions, the loading strategy developed here, was compared to other loading strategies found in literature. The purpose of this comparison is to highlight how commonly employed loading

strategies can produce strain distributions which differ significantly from experimental strain measurements. A comparison of strain distributions for different loading strategies is shown in Figure 5, showing the axial strain in the 37% slice. As is apparent, the three loading strategies produce very different strain distributions. The mean error for load strategy 1 is 2.5%, while the error for load strategy 2 and 3 increase dramatically to 31.6% and 47.9% respectively. The neutral axis is also seen to shift for the different loading strategies. The neutral axis sits at an angle of −56.7° for load strategy 1, this increases to −45.9° for load strategy 2, and −25.8° for load strategy 3. As the neutral axis rotates, so too does the strain distribution. For example, in load strategy 1, the peak axial strain occurs in the tibial ridge, while in load strategy 3 the axial peak strain occurs on the antero-medial surface. This further demonstrates the importance of experimental calibration of the loading strategy. Further, this highlights that caution should be used when interpreting results of FE models which have not calibrated the loading conditions as these may not match the true *in vivo* case.

3.4 Limitations

While strain gauges are a standard approach to assess tibial strains (De Souza et al., 2005; Sugiyama et al., 2008; Patel et al., 2014), there are some limitations which should be noted. First, strain gauges are applied to a surface, and thus provide an average strain over that surface. For the mouse tibia, it has been shown that surface strains can be highly variable (Carriero et al., 2014). A second limit of strain gauging is the induced stiffening effect. The addition of a strain gauge and glue to the tibial surface will increase the stiffness of the tibia.

This study used three strain gauges which would enhance the stiffening effect. Begonia *et al.* (2015) explored the stiffening effect in the mouse ulna, finding the addition of a strain gauge increased the ulna stiffness by 24%. While a similar study has not been conducted in the tibia, it is likely that the stiffening effects is less significant. As justification, it should be noted that the tibia 37% section (attachment site in this study) is much larger than the ulna midsection (attachment site in Begonia et al. (2015)), having approximately 3× the cortical area and 17× the polar moment of area (Sugiyama et al., 2008). Thus, the stiffening effect in the tibia would be less than that of the ulna. Finally, direct contact of the strain gauge and surface can be challenging for small curved surfaces (like in the tibia), leading to a layer of glue between the gauge and surface; this may reduce the gauge accuracy. Such a gap was observed in this study (see Figure 1). However, as argued in Section 3.2, the three gauge problem solved in this study is overdetermined. As the error successfully minimised, this adds certainty to our approach and assumptions.

While strain gauging is the most common technique for evaluating strains in the mouse tibia loading model, other techniques such as digital image correlation (DIC) (Carriero et al., 2014; Begonia et al., 2015) and digital volume correlation (DVC) (Giorgi and Dall'Ara, 2018) should be highlighted. Both DIC and DVC are non-contact methods employing image based techniques to evaluate strains. Both approaches have the advantages of not involving a stiffening effect and allowing for evaluation of a strain distribution (rather than an averaged strain value as with gauges). These methods could thus provide an alternate means for calibrating the loading conditions in the mouse tibia compression model.

Another potential limitation is the partial volume effect which presents in digital microscopy techniques such as μCT. For trabecular bone, with a thickness of approximately 45 μm (Sugiyama et al., 2010), the 21 μm voxel size could result a low-fidelity representation. However, Oliverio *et al.* (2017) demonstrated that trabecular has little effect on the overall mechanics of the mouse tibia, thus it is unlikely that this would influence the strain distribution at the gauge locations. For cortical bone, with a thickness between approximately 150 – 300 μm (Pereira et al., 2015), this could have influenced the overall stiffness of the tibiae. However, as the voxel size was several factors larger than the cortical thickness, this is likely minimal. The partial volume effect was also moderated by using an Otsu threshold which automatically selects a threshold level which maximises the inter-class variance between the bone and background.

4 Conclusion

In summary, this work developed a novel, experimentally informed method for applying load to the tibial plateau in FE models of the murine tibia compression model. To achieve this, the complex load distribution on the tibial plateau was idealised as a single point load acting at an equivalent location. Strains in the tibia were modelled via FE, and compared to *ex vivo* strain values from three surfaces of the tibia. The equivalent load location was determined by minimising the error between *ex vivo* and FE strains. As expected, the equivalent load location was found to be on the posterior edge of the condyle. However, the load location was found to vary between specimens. To demonstrate the significance of this technique, three different loading strategies were investigated, and it was shown that strains in the tibia were highly sensitive to the load location. For *in vivo* tests, it is suggested that the equivalent load location will vary across specimens and with experimental factors such as hindlimb alignment and flexion. As such, future studies may consider the multi-gauge technique developed here to identify the equivalent load location, allowing for improved FE modelling.

Supplementary Material

Refer to Web version on PubMed Central for supplementary material.

Acknowledgements

This work was supported by ARC discovery project DP180103009, and U.S. NIH/NIAMS grants R01 AR047867 and P30 AR057235. We gratefully acknowledge Mr. Tarpit Patel for μCT scan acquisition, and the High-Performance Computing (HPC) resources provided by the Queensland University of Technology.

References

Albiol L, Cilla M, Pflanz D, Kramer I, Kneissel M, Duda GN, Willie BM, and Checa S (2019). Sost deficiency leads to reduced mechanical strains at the tibia midshaft in strain-matched in vivo loading experiments in mice. Journal of The Royal Society Interface, 15(141):20180012.

Begonia MT, Dallas M, Vizcarra B, Liu Y, Johnson ML, and Thiagarajan G (2015). Non-contact strain measurement in the mouse forearm loading model using digital image correlation (dic). Bone, 81:593–601. Epigenetic Mechanisms Regulating Bone Biology and Pathology. [PubMed: 26388521]

Borges PDN, Forte A, Vincent T, Dini D, and Marenzana M (2014). Rapid, automated imaging of mouse articular cartilage by microct for early detection of osteoarthritis and finite element modelling of joint mechanics. Osteoarthritis and Cartilage, 22(10):1419–1428. Special Themed Issue - Imaging in Osteoarthritis. [PubMed: 25278053]

Carriero A, Abela L, Pitsillides AA, and Shefelbine SJ (2014). Ex vivo determination of bone tissue strains for an in vivo mouse tibial loading model. Journal of Biomechanics, 47(10):2490–2497. [PubMed: 24835472]

Carriero A, Pereira A, Wilson A, Castagno S, Javaheri B, Pitsillides A, Marenzana M, and Shefelbine S (2018). Spatial relationship between bone formation and mechanical stimulus within cortical bone: Combining 3d fluorochrome mapping and poroelastic finite element modelling. Bone Reports, 8:72–80. [PubMed: 29904646]

Christiansen BA, Bayly PV, and Silva MJ (2008). Constrained tibial vibration in mice: A method for studying the effects of vibrational loading of bone. Journal of Biomechanical Engineering, 130(4):044502–044502–6.

De Souza RL, Matsuura M, Eckstein F, Rawlinson SC, Lanyon LE, and Pitsillides AA (2005). Non-invasive axial loading of mouse tibiae increases cortical bone formation and modifies trabecular organization: A new model to study cortical and cancellous compartments in a single loaded element. Bone, 37(6):810–818. [PubMed: 16198164]

Fritton JC, Myers ER, Wright TM, and van der Meulen MC (2008). Bone mass is preserved and cancellous architecture altered due to cyclic loading of the mouse tibia after orchidectomy. Journal of Bone and Mineral Research, 23(5):663–671. [PubMed: 18433300]

Frost HM (2003). Bone's mechanostat: A 2003 update. Anat. Rec, 275A(2):1081–1101.

Giorgi M and Dall'Ara E (2018). Variability in strain distribution in the mice tibia loading model: A preliminary study using digital volume correlation. Medical Engineering & Physics, 62:7–16. [PubMed: 30243888]

Goff M, Chang K, Litts E, and Hernandez C (2014). The effects of misalignment during in vivo loading of bone: Techniques to detect the proximity of objects in three-dimensional models. Journal of Biomechanics, 47(12):3156–3161. [PubMed: 25001204]

Imhauser C, Mauro C, Choi D, Rosenberg E, Mathew S, Nguyen J, Ma Y, and Wickiewicz T (2019). Abnormal tibiofemoral contact stress and its association with altered kinematics after center-center anterior cruciate ligament reconstruction: An in vitro study. Am J Sports Med, 41(4):815–825.

Lynch ME, Main RP, Xu Q, Schmicker TL, Schaffler MB, Wright TM, and van der Meulen MC (2011). Tibial compression is anabolic in the adult mouse skeleton despite reduced responsiveness with aging. Bone, 49(3):439–446. [PubMed: 21642027]

Main RP, Shefelbine SJ, Meakin LB, Silva MJ, van der Meulen MCH, and Willie BM (2020). Murine axial compression tibial loading model to study bone mechanobiology: Implementing the model and reporting results. Journal of Orthopaedic Research, 38(2):233–252. [PubMed: 31508836]

Moustafa A, Sugiyama T, Prasad J, Zaman G, Gross TS, Lanyon LE, and Price JS (2012). Mechanical loading-related changes in osteocyte sclerostin expression in mice are more closely associated with the subsequent osteogenic response than the peak strains engendered. Osteoporosis International, 23(4):1225–1234. [PubMed: 21573880]

Oliviero S, Lu Y, Viceconti M, and Dall'Ara E (2017). Effect of integration time on the morphometric, densitometric and mechanical properties of the mouse tibia. Journal of Biomechanics, 65:203–211. [PubMed: 29126603]

Otsu N (1979). A threshold selection method from gray-level histograms. IEEE Transactions on Systems, Man, and Cybernetics, 9(1):62–66.

Patel TK, Brodt MD, and Silva MJ (2014). Experimental and finite element analysis of strains induced by axial tibial compression in young-adult and old female c57bl/6 mice. Journal of Biomechanics, 47(2):451–457. [PubMed: 24268312]

Pereira AF, Javaheri B, Pitsillides AA, and Shefelbine SJ (2015). Predicting cortical bone adaptation to axial loading in the mouse tibia. Journal of The Royal Society Interface, 12(110):20150590.

Razi H, Birkhold AI, Zaslansky P, Weinkamer R, Duda GN, Willie BM, and Checa S (2015). Skeletal maturity leads to a reduction in the strain magnitudes induced within the bone: A murine tibia study. Acta Biomaterialia, 13:301–310. [PubMed: 25463494]

Razi H, Birkhold AI, Zehn M, Duda GN, Willie BM, and Checa S (2014). A finite element model of in vivo mouse tibial compression loading: influence on boundary conditions. Facta Universitatis, Series: Mechanical Engineering, 12(3):195–207.

Rosa N, Simoes R, Magalhães FD, and Marques AT (2015). From mechanical stimulus to bone formation: A review. Medical Engineering & Physics, 37(8):719–728. [PubMed: 26117332]

Saxon LK, Jackson BF, Sugiyama T, Lanyon LE, and Price JS (2011). Analysis of multiple bone responses to graded strains above functional levels, and to disuse, in mice in vivo show that the human lrp5 g171v high bone mass mutation increases the osteogenic response to loading but that lack of lrp5 activity reduces it. Bone, 49(2):184–193. [PubMed: 21419885]

Stadelmann VA, Hocké J, Verhelle J, Forster V, Merlini F, Terrier A, and Pioletti DP (2009). 3d strain map of axially loaded mouse tibia: a numerical analysis validated by experimental measurements. Computer Methods in Biomechanics and Biomedical Engineering, 12(1):95–100. [PubMed: 18651261]

Sugiyama T, Price JS, and Lanyon LE (2010). Functional adaptation to mechanical loading in both cortical and cancellous bone is controlled locally and is confined to the loaded bones. Bone, 46(2):314–321. [PubMed: 19733269]

Sugiyama T, Saxon LK, Zaman G, Moustafa A, Sunters A, Price JS, and Lanyon LE (2008). Mechanical loading enhances the anabolic effects of intermittent parathyroid hormone (1–34) on trabecular and cortical bone in mice. Bone, 43(2):238–248. [PubMed: 18539556]

Willie BM, Birkhold AI, Razi H, Thiele T, Aido M, Kruck B, Schill A, Checa S, Main RP, and Duda GN (2013). Diminished response to in vivo mechanical loading in trabecular and not cortical bone in adulthood of female c57bl/6 mice coincides with a reduction in deformation to load. Bone, 55(2):335–346. [PubMed: 23643681]

Yang H, Butz KD, Duffy D, Niebur GL, Nauman EA, and Main RP (2014). Characterization of cancellous and cortical bone strain in the in vivo mouse tibial loading model using microct-based finite element analysis. Bone, 66:131–139. [PubMed: 24925445]

Zhang K, Li L, Yang L, Shi J, Zhu L, Liang H, Wang X, Yang X, and Jiang Q (2019). The biomechanical changes of load distribution with longitudinal tears of meniscal horns on knee joint: a finite element analysis. Journal of Orthopaedic Surgery and Research, 14(1):237. [PubMed: 31345248]

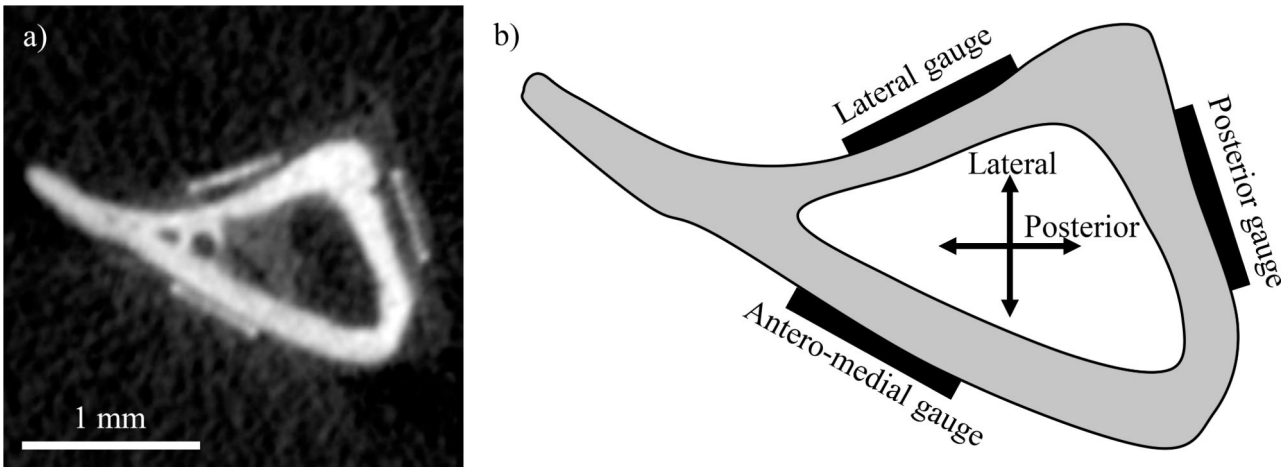

Figure 1:
a) μCT scan slice located 37% along the tibia (proximal to distal) showing the attached strain gauges. b) Corresponding schematic showing strain gauge labelling and anatomical directions.

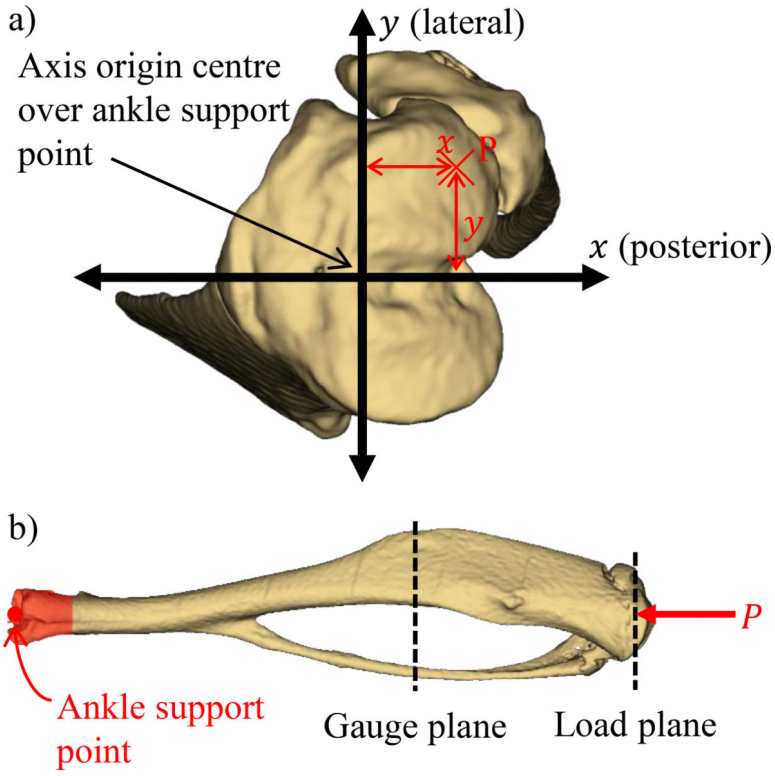

Figure 2:
BCs of the FE model. a) The coordinate system centred over the ankle support point with a compressive load P acting at a coordinate (x,y). b) The location of the load plane and the ankle support point. The load plane is located at the 3% position (proximal to distal). The ankle support point is located at the centre of the inferior articular surface, with nodes of the lower 10% of the tibia constrained to the ankle support point.

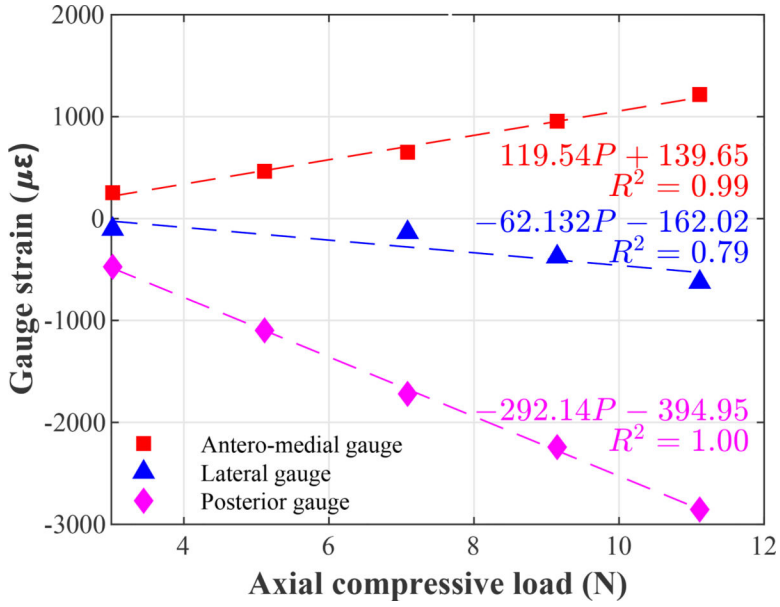

Figure 3:
Strain gauge readings from ex vivo compressive loading of specimen 1.

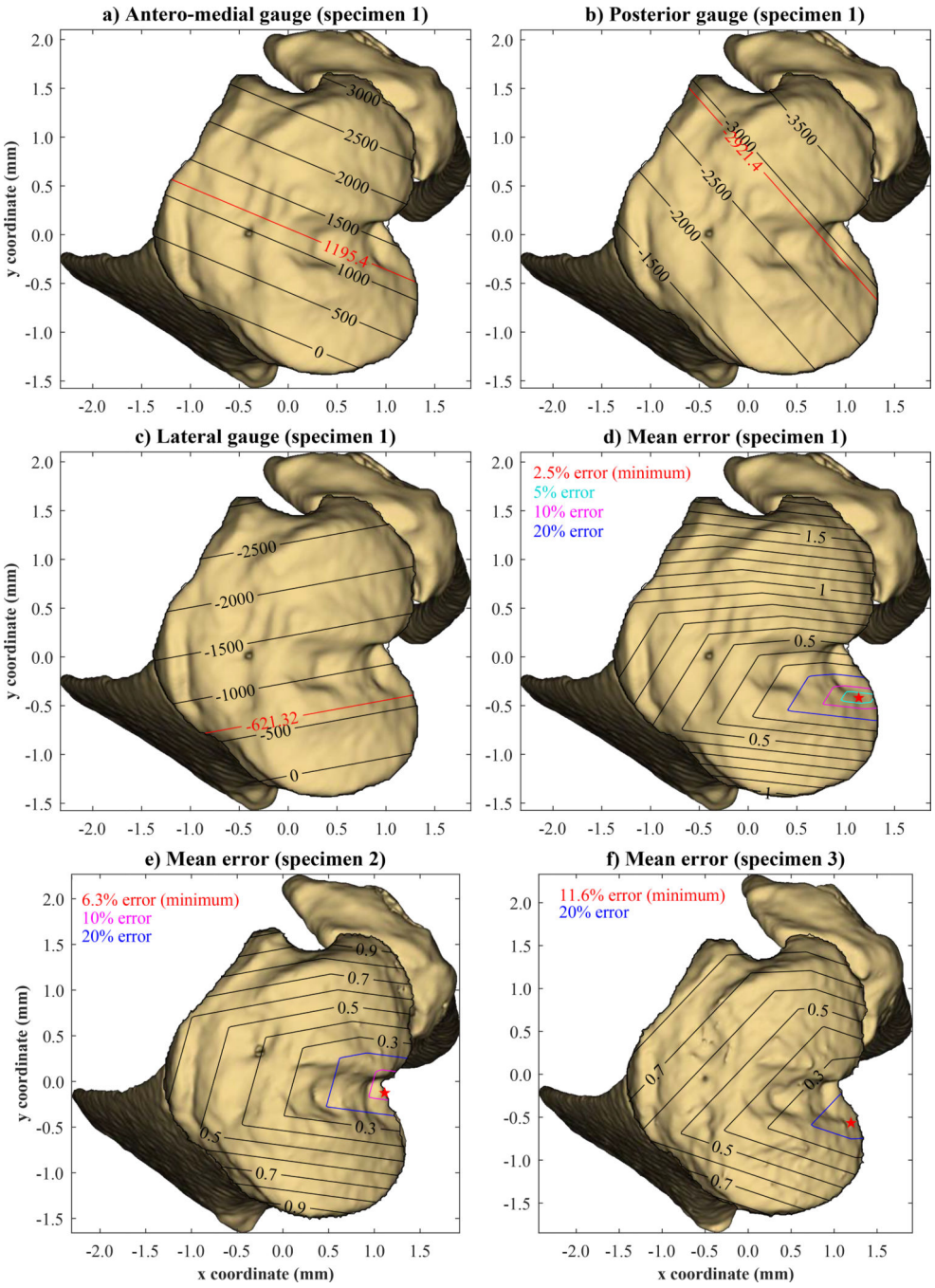

Figure 4:

Influence of load location on the FE strains measured at the a) antero-medial, b) posterior, and c) lateral gauge locations using a compressive load of 10 N for specimen 1. The load location is measured relative to the ankle coordinate. The black contours show the strain reading at the relevant gauge in με. The red line indicated where the in silico strain reading matches the experimental measurements, these being 1195.4 με, −2921.4 με, and −621.32 με respectively. The mean relative error between the experimental and FE strains for a given

load location is shown for specimen 1 – 3 in d) – f) respectively, additionally the point of minimum error is identified (i.e. load location).

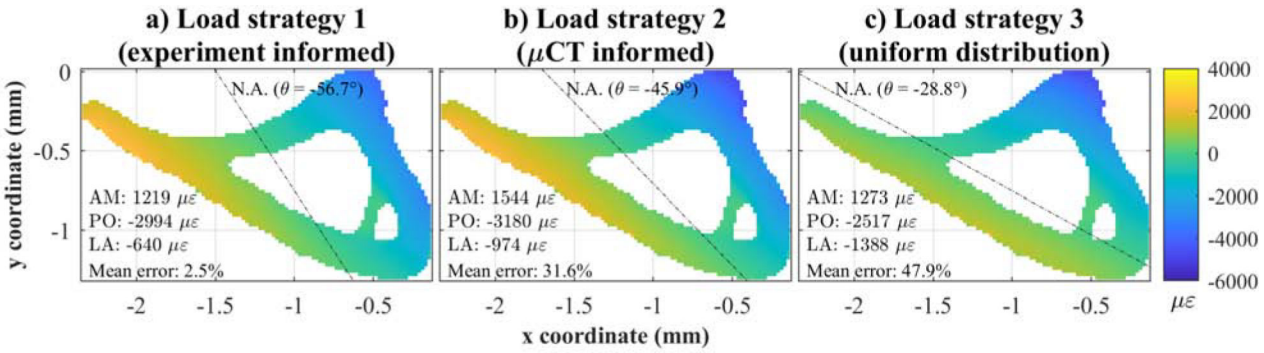

Figure 5:

Comparison of the axial strain on the 37% slice for the three loading strategies for specimen 1. The strains at the antero-medial (AM), posterior (PO) and lateral (LA) gauges are shown, along with the mean error between the gauge readings from the FE model and ex vivo loading. The neutral axis (N.A.) is also indicated. a) Load strategy 1 – load applied at the equivalent point load determined in this study. b) Load strategy 2 – load applied to the posterior edge of each condyle. c) Load strategy 3 – load evenly distributed over the tibial plateau.